Estimates of the Vertical Wavenumber–Frequency Spectra of Vertical Shear and Strain

JEFFREY T. SHERMAN AND ROBERT PINKEL

Marine Physical Laboratory, Scripps Institution of Oceanography, University of California, San Diego, La Jolla, California

(Manuscript received 29 September 1989, in final form 13 August 1990)

ABSTRACT

Measurements of vertical shear and strain were acquired from the research platform *FLIP* during the PATCHEX experiment in October, 1986 (34°N, 127°W). Vertical shear was observed from two separate Doppler sonar systems. A long-range sonar, with independent estimates every 18 m, sampled from 150–1200 m in depth. A short-range sonar measured fine-scale shear over 150–180 m depth, with 1.5 m vertical resolution. Vertical strain, $\partial\eta/\partial z$, was estimated from two repeatedly profiling CTDs. These sampled to 560 m once every three minutes. The time variation of the strain field is monitored in both Eulerian (fixed-depth) and semi-Lagrangian (isopycnal-following) reference frames, from 150–406 m depth.

Eulerian vertical wavenumber–frequency (m, ω) spectra of vertical shear and strain exhibit a frequency dependency which is a strong function of wavenumber (ω^{-2}-ω^{0} for m = 0.01–0.3 cpm). In contrast, the semi-Lagrangian strain spectrum is more nearly separable in frequency and wavenumber, in closer agreement with the Garrett–Munk (GM) internal wave spectral model.

When a simulated GM shear field is vertically advected by a GM isopycnal displacement field, the resultant Eulerian vertical wavenumber–frequency spectrum exhibits the same qualitative, nonseparable, form as the PATCHEX shear spectrum: The dominant near-inertial waves are Doppler-shifted across all frequency bands, resulting in a "white" frequency spectrum at high wavenumbers. Measured ratios of Eulerian shear/strain variance support this interpretation. High shear-low strain variances (characteristic of near-inertial waves) are seen at high wavenumber, high encounter frequencies. The conclusion is that internal wave vertical self-advection strongly alters the observed frequency at high vertical wavenumbers in an Eulerian reference frame.

1. Introduction

This paper explores the frequency (ω)–vertical wavenumber (m) spectra of vertical shear and strain. Spectral estimates are based on a 7.5 day dataset of shear ($\partial u/\partial z, \partial v/\partial z$, where u, v are horizontal velocity) and strain ($\partial\eta/\partial z \equiv \eta_z$, where η is isopycnal displacement). The data were collected during the PATCHEX experiment (October 1986), located in the eastern North Pacific (34°N, 127°W). Field work was done from the research platform *FLIP*, which was two-point moored for the duration of the data collection. Vertical strain is estimated from two profiling CTDs, which sampled the top 560 m of the water column. The shear field was observed with two different Doppler sonars. A long range pulse-to-pulse incoherent sonar provides large-scale information (over 1 km depth, with independent estimates every 18m). A short-range pulse-to-pulse coherent sonar yields fine-scale shear structure (30 m depth coverage, with 1.5 m vertical resolution).

Spectral estimates of vertical shear $\Phi(\omega, m)$ and strain $\Gamma(\omega, m)$ are presented in sections 4 and 5 respectively. Here $\Gamma(\omega, m)$ is estimated in both an Eulerian (fixed-depth) reference frame and a "semi-Lagrangian" coordinate system, where η_z is measured while vertically tracking isopycnals. This approach removes the effects of vertical advection. The 30 m stationary aperture of the short-range sonar does not allow fine-scale shear to be adequately tracked while following isopycnals Information is lost when an isopycnal travels outside the 30 m window. This constraint limits $\Phi(\omega, m)$ to the Eulerian reference frame. Variances of Eulerian shear and strain from different (ω, m) bands are compared to linear internal wave theory (section 6). Results suggest that low-frequency waves are Doppler-shifted to higher encounter frequencies in an Eulerian reference frame. This is confirmed in a simulation study where a Garrett–Munk internal wave spectrum is both vertically and horizontally self-advected past an array of fixed-depth sensors (section 7).

2. Background

Fine-scale shear is thought to play a key role in the dissipation of the internal wave field, leading to the production of microscale mixing in the sea. Yet, little is known about the space–time variability of the shear field. What is the time dependence of those motions which influence the evolution of low Richardson number events? How does the energy distribution in fre-

Corresponding author address: Dr. Jeffrey Sherman, 0230, Scripps Institution of Oceanography, La Jolla, CA 92093.

quency vary from low wavenumbers, where motions are thought to behave as linear internal waves, to high wavenumbers, where strong nonlinearities are expected (Holloway 1980)? Modelers have used the Garrett–Munk (GM) (Garrett and Munk 1972, 1975, 1979; Munk 1981) spectrum to estimate statistics of mixing events (e.g., Desaubies and Smith 1982). The GM model is synthesized from a variety of one-dimensional spectral measurements. These are assimilated under the assumption that the spectrum is separable: all frequencies share the same wavenumber dependence. Is this an accurate assumption?

Based on shear measurements from a variety of vertical profiling instruments, Gargett et al. (1981) have proposed a vertical wavenumber spectral model which has an m^0 slope at low wavenumbers, with a depth-independent rolloff to a m^{-1} slope at $m_c \approx 0.1$ cpm (Fig. 1). Following the work of Munk (1981), Gargett et al. suggest that the rolloff occurs when the inverse Richardson function (Ri^{-1}) reaches a value of 1, where

$$\mathrm{Ri}^{-1}(m) = \frac{1}{N^2}\int_0^m \Phi(m)dm. \qquad (1)$$

Here, N is the buoyancy frequency, and $\Phi(m)$ is the vertical wavenumber spectrum of shear. Given the cannonical energy level of the GM model, Munk (1981) suggests $\mathrm{Ri}^{-1}(m_c) = 0.5$. More recently, Duda and Cox (1989) have observed shear spectra with large variations in kinetic energy. These spectra fail to conform to any simple shape, but nevertheless tend to have Ri^{-1} (0.1 cpm) $\approx$ 1–3. Kunze et al. (1990) have suggested $m^{-1.4}$ slope at $m > 0.1$ cpm as a better analytic fit to several different datasets.

Both the Gargett et al. (1981) and Duda and Cox (1989) measurements are from slow-profiling instruments. These cannot describe the shear's temporal characteristics. The GM assumption is that the wavenumber spectral shape is independent of frequency. All frequency components of the shear spectrum should replicate the Gargett et al. model. However, the only published measurement of $\Phi(\omega, m)$ (Pinkel 1985, Fig. 2a) indicates a wavenumber spectral shape strongly dependent on frequency out to $m = 0.03$ cpm. Pinkel's analysis is in a fixed-depth coordinate system. To what extent does vertical self-advection influence the spectral estimate?

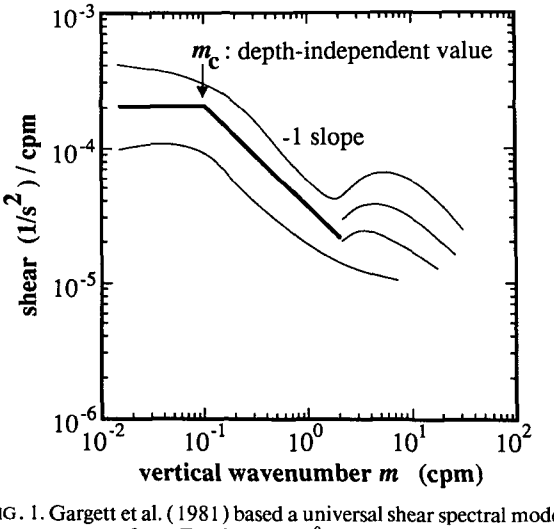

FIG. 1. Gargett et al. (1981) based a universal shear spectral model on measurements from FAME. The m^0 slope at low wavenumbers has its energy level scale in a WKB fashion as N^2. The break in slope at $m_c \approx 0.1$ cpm is thought to be a depth-independent parameter occurring when $\mathrm{Ri}^{-1}(m_c) = 1$. The m^{-1} slope is then followed by an intermittent high-wavenumber region, dependent upon mixing events.

3. Observations

During October 1986 the research platform *FLIP* participated in the PATCHEX experiment at 34°N, 127°W, approximately 600 km west of Point Conception, California. *FLIP* was kept on station by a taut two-point mooring. Relative bearing remained constant to within ±5° for most of the data acquisition period. Wind shifts occasionally produced excursions as great as 15°. Light winds were experienced for most of the cruise, with wind speeds rarely exceeding 7 m s^{-1}.

FLIP is instrumented with two Sea-Bird Electronics Model SBE-9 CTDs, two distinct Doppler sonar systems, and a variety of environmental sensors. One CTD profiles between 0 and 300 m, the other from 260–560 m (Fig. 3). The CTD drop rate is 3.8 m s^{-1}. A complete cycle was completed every three minutes. Conductivity and temperature resolution are 5×10^{-4} mmho/cm^{-1}, and 5×10^{-4} °C. To avoid wake disturbances caused by the package itself, data are recorded only while the instruments descends. Approximately ten thousand profiles were obtained over a three week period of continuous operation.

Salinity spiking is reduced by matching the conductivity sensor time response to that of the temperature sensor. The method used is similar to Williams (1985). Briefly stated, a low salinity-gradient region is chosen such that the conductivity sensor is mainly responding to temperature. Cross-spectra are calculated between dC/dz and dT/dz, giving a phase and amplitude transfer function. This correction is applied to dC/dz for each profile. A low-pass filter having a 3 dB rolloff at ~0.5 cpm is also applied to both dC/dz and dT/dz. The gradient profiles are then reintegrated. Salinity, potential temperature, and potential density are calculated for every profile.

Four long-range Doppler sonars, using pulse-to-pulse incoherent processing, measure the oceanic velocity field to one km depth. A four-beam short-range Doppler sonar, using pulse-to-pulse coherent processing, measures fine-scale shear from 150–180 m (Sherman 1989).

The long-range sonar operates at 75 kHz, with beams oriented downwards at 52°. Thirty-millisecond pulses

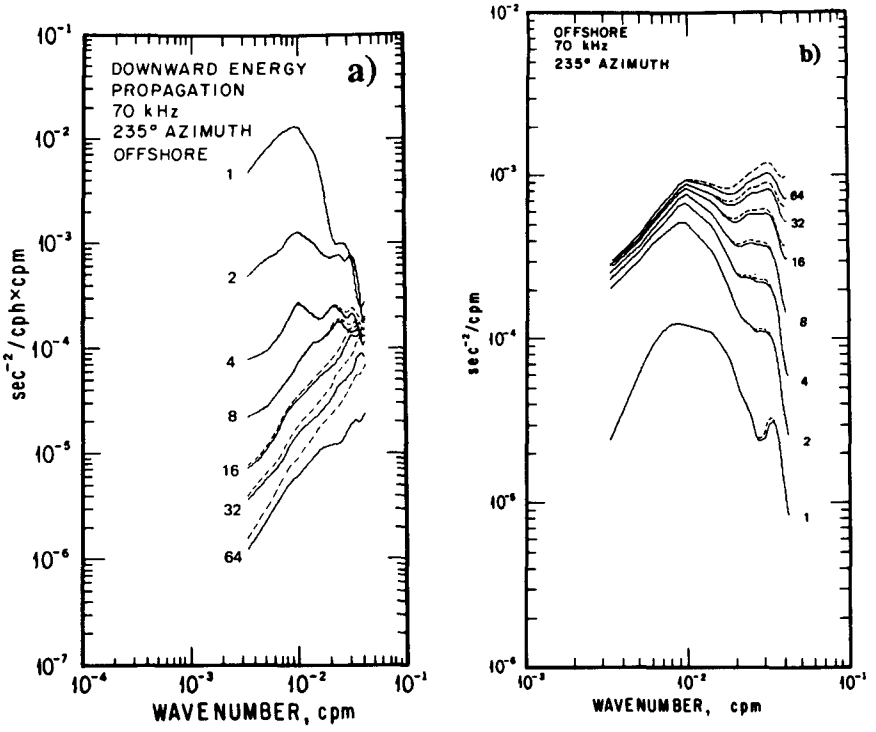

FIG. 2. (a) Cross sections of $\Phi(\omega, m)$ are shown for 1, 2, 4, 8, 16, 32 and 64 cpd, as calculated by Pinkel (1985). Dashed lines are the measured values, while the solid lines represent estimates after modeled instrument noise has been removed. (b) When $\Phi(\omega, m)$ is integrated in frequency, the cumulative shear spectrum is obtained. Each line represents the shear variance integrated from 0.5 cpd up to the labeled value (i.e., 0.5–1.0 cpd). The resulting spectral shape (m^0 slope for $m > 0.01$ cpm) is in agreement with the Gargett et al. (1981) model.

are transmitted, yielding independent velocity estimates every 18 m. The return signal/noise ratio exceeds unity to depths in excess of 1 km. However, to avoid the necessity of correcting velocity biases, which occur at low signal-to-noise ratio (Plueddemann 1987), only velocity estimates from 150–750 m are used in the present analysis. Although a 22 day dataset was obtained in PATCHEX, only a 6.4 day subset overlapping the short-range sonar's time series is presently discussed. Pinkel et al. (1987) give a more complete description of the long-range sonar system.

The short-range Doppler sonar operates at 160 kHz, with four beams pointed downwards at 55°. It employs pulse-to-pulse coherent processing. The Doppler shift is estimated from the phase variation of the return signal, as measured from pulse to pulse (cf. Lhermitte and Serafin 1984). Coherent processing gives better spatial resolution and velocity precision relative to incoherent processing, at the expense of limiting maximum range. During PATCHEX, the short-range sonar transmitted a 1 ms pulse every 60 ms, resulting in 0.6 m vertical sampling resolution over 30 m depth. The first 6 meters of the return are not usable due to degradation of the signal by near-field effects.

The short-range sonar is suspended from *FLIP*'s port boom at a depth of 144 m. To remove the effect of Doppler-smearing by time variations in instrument motion, velocity differences in range are estimated, rather than velocity itself. This technique effectively provides vertical shear estimates directly. Vertical wavenumber shear spectra exhibit a white noise floor at $m \approx 0.3$ cpm, indicating a useful vertical resolution of 1.5 m. The PATCHEX time series extends over a 7.5 day period.

Both the long-range and short-range sonars consist of two pairs of down-looking back-to-back beams, allowing both components of horizontal velocity to be resolved. A Doppler sonar measures the component of water velocity parallel to the beam. If back-to-back beams are oriented north–south (N–S) at angle θ relative to the vertical, then the measured beam velocities (v_N, v_S) are

$$v_N = u_N \sin\theta + w \cos\theta, \quad v_S = -u_N \sin\theta + w \cos\theta \tag{2}$$

where u_N, w are the north and vertical components of the velocity field; u_N and w can be calculated by subtracting or adding v_N and v_S. If a second pair of back-to-back beams is not coplanar with the first, all three

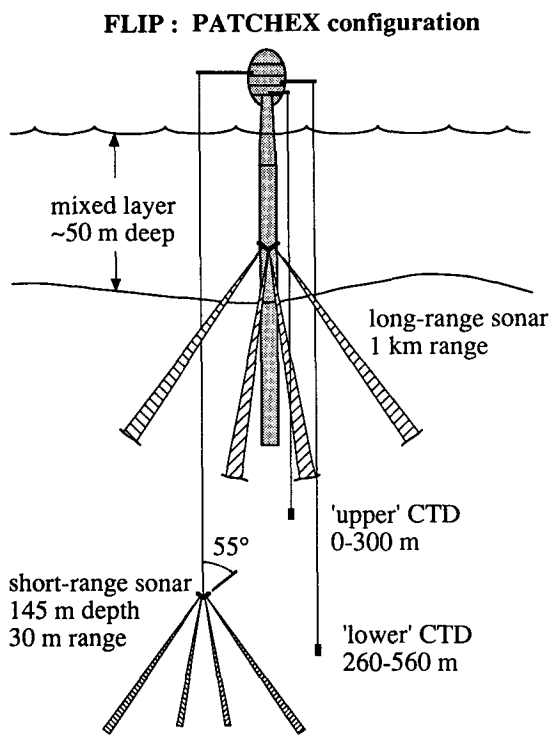

FIG. 3. During the PATCHEX experiment *FLIP* was configured with two rapid profiling CTDs, a four beam long-range, pulse-to-pulse incoherent Doppler sonar, and a four beam, pulse-to-pulse coherent Doppler sonar. Also on board were two surface wave/mixed layer sonars, and a full complement of environmental sensors (not shown).

components of the velocity field can be estimated. In this work, shear is derived from the estimated horizontal velocities. Horizontal variation in the velocity field across the beam separation distance will result in error in the estimates (see Appendix). This problem is of lesser consequence for the fine scale measurements from the coherent sonar, as the beams are separated by less than 30 m horizontally. The high wavenumber shear estimates obtained from the long range sonar are more strongly influenced by lateral variability, with high-frequency variance underestimated by perhaps as much as 50%.

4. Vertical shear

The 7.5 day shear time series from the short-range sonar has been divided into seven subsets of 44 hour duration, with 50% overlap between subsets. The data are Fourier transformed in depth and time, with a triangular data window applied in both dimensions. The vertical wavenumber–frequency spectral estimate, $\Phi(\omega, m)$, is formed by averaging the squared Fourier coefficients over the seven subsets (four independent); $\Phi(\omega, m)$ is divided into six frequency bands: 44–16, 16–8, 8–4, 4–2, 2–1, and 1–0.7 hour periods. The average spectral energy density is calculated for each frequency band (Fig. 4a).

Similar spectral estimates of the low wavenumber portion of $\Phi(\omega, m)$ are formed from the long-range sonar data. A 6.4 day time series coincident with the short-range sonar data has been subdivided into seven subsets of 38.4 hour duration, with 50% overlap between subsets. Here $\Phi(\omega, m)$ is estimated following the same procedure as for the short-range sonar (triangle windowing, Fourier transformation, and averaging over the seven spectral estimates and six frequency bands). Spectral levels from the long-range sonar have been adjusted to provide an optimal fit with the short-range sonar spectrum. This adjusted level is ~40% lower than the value suggested using WKB theory. In the WKB approximation, vertical shear spectral density should vary as N^2, where N is the local buoyancy frequency. Given the observed depth-averaged values of N for the two sonar systems (=5.3 cph for 150–180 m, 2.6 cph for 150–750 m), the long-range sonar's spectral level should be increased by a factor of ~4.2 to match the short range measurements. A best fit occurs with a rescaling factor of 2.5. Applying the WKB theory may be inappropriate at such a shallow depth, as the buoyancy frequency is no longer slowly-varying in the upper thermocline. This is consistent with Gregg's (1989) PATCHEX observations of average shear variance with depth (his Fig. 1). He shows disagreement with WKB scaling beginning at ~200 m. Gregg's shear variance decreases to half the expected WKB value by 100 m.

The PATCHEX spectral shape that emerges is reminiscent of Pinkel's (1985) spectrum, reproduced here in Fig 2. High frequencies are band-limited in wavenumber. The center of the band shifts to higher wavenumber at higher frequencies. Spectral density converges to the same energy level at high wavenumbers, such that high wavenumber motions appear "white" in frequency (Fig. 4b). The GM assumption of separability is strongly violated. When the PATCHEX wavenumber spectrum is integrated over all frequencies (Fig. 4d), good agreement is seen with the Gargett et al. model, and Pinkel's (1985) measurements (Fig. 2b). The high-wavenumber rolloff has a slope between m^{-1} and m^{-2}, dependent upon the modeled noise correction scheme applied. Estimates with noise removed are shown in Fig. 4a as dashed lines.

5. Vertical strain

The PATCHEX density profiles are converted to estimates of vertical strain in both Eulerian and "semi-Lagrangian" (isopycnal-following) coordinates. The Eulerian strain is defined here to be the ratio of the instantaneous density gradient to the time averaged gradient at each depth of interest. This definition preserves the type of "fine-structure contamination" experienced by the Doppler sonars. Alternate definitions of Eulerian strain can be formed which are unaffected

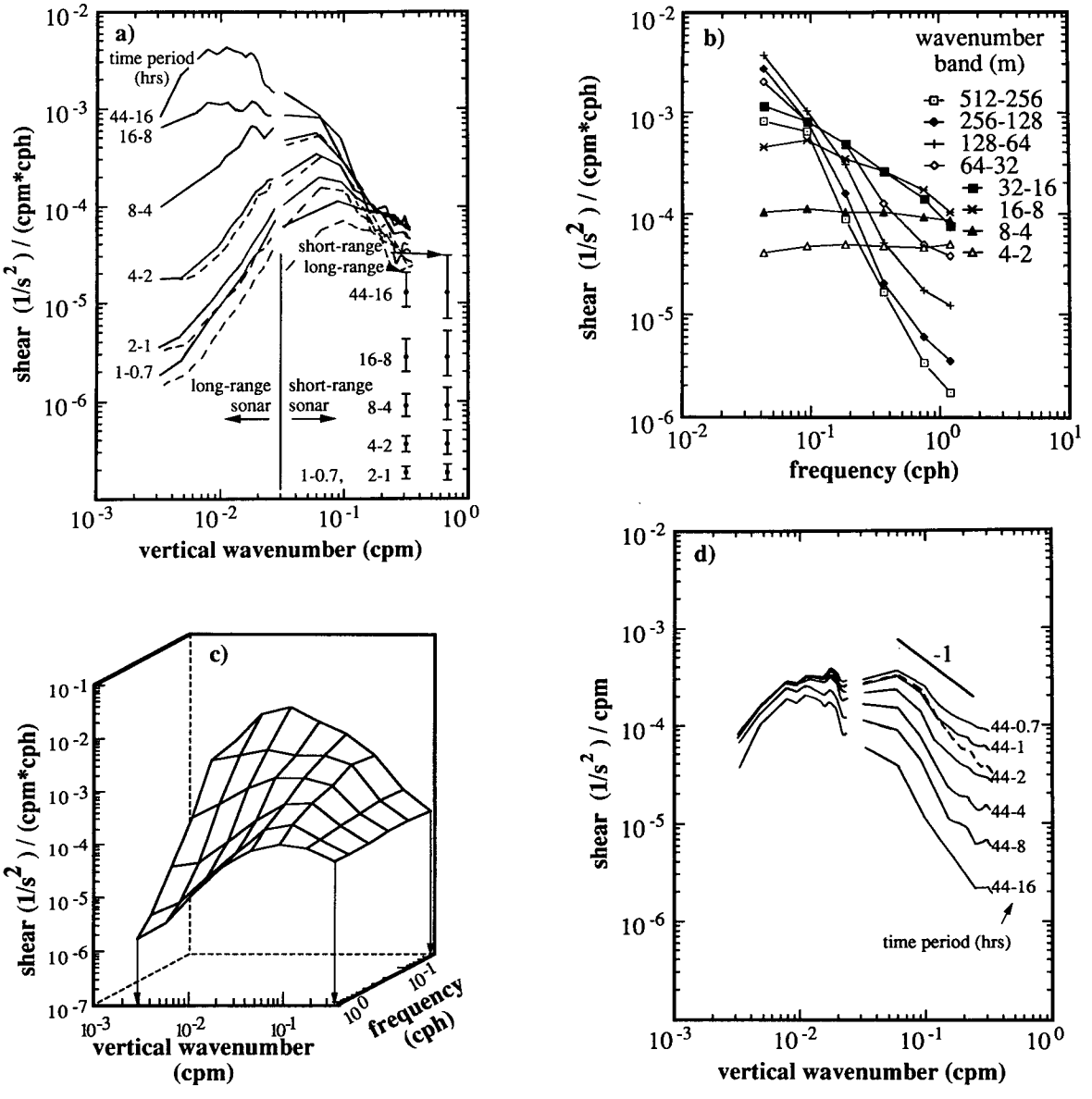

FIG. 4. (a) The PATCHEX composite $\Phi(\omega, m)$ includes both the long-range and short-range sonar estimates. Average spectral density levels are shown for six bands: 44–16, 16–8, 8–4, 4–2, 2–1, and 1–0.7 hour periods. 95% confidence limits are shown for each band. Cross sections of $\Phi(\omega, m)$ are displayed for both sonars. The long-range sonar's spectral levels have been reduced by 40% from WKB theory to provide the optimum fit to the short-range sonar spectrum. Dashed lines represent the resultant spectrum when modeled noise is removed. (b) The same spectrum is now viewed in frequency, with cross-sections displayed for eight different wavenumber bands (as labeled). Each line represents the average spectral density for its wavenumber band. (c) A three-dimensional view of $\Phi(\omega, m)$. (d) Integration of energy across frequency bands yields a cumulative vertical-wavenumber spectrum, with the top curve representing total energy contained between 44–0.7 hour periods. The dashed line is the 44–0.7 band as computed when modeled noise is removed.

by the vertical advection of "frozen" features in the background gradients (Williams 1985; Pinkel et al. 1991).

Using the same set of density profiles, a corresponding set of reference densities is selected such that the mean separation between adjacent isopycnals equals 1 m for the 21 day period. The depth of occurrence of these densities is tracked as a function of time. This allows the effect of vertical advection (but not horizontal) to be distinguished from the time evolution of the strain field. In the semi-Lagrangian frame, strain is defined as the ratio of instantaneous to mean isopycnal separation, minus one. Temporal variations of the strain are tracked as a function of density, with

isopycnal mean (but not instantaneous) positions being equally separated in depth.

The vertical wavenumber–frequency strain spectrum, $\Gamma(\omega, m)$, is calculated from a 7.5 day data subset (overlapping the short-range sonar's time series) spanning 150–406 m. A triangular window is applied in depth and time, followed by the Fourier transform. The squared Fourier coefficients are averaged into the same six frequency bands as the shear spectrum. Estimates of $\Gamma(\omega, m)$ as seen in both the Eulerian and semi-Lagrangian frames are shown in Figs. 5 and 6. The Eulerian strain spectrum is similar to the shear spectrum. There is a shift of the cutoff wavenumber m_c and a narrowing of the wavenumber bandwidth with increasing frequency. All frequencies converge to the same spectral level at high wavenumber. The cumulative strain spectrum (Fig. 5b) is also similar to the shear spectrum (Fig. 4d).

The semi-Lagrangian vertical stain spectrum has quite different characteristics. The frequency spectrum is red even at high wavenumbers. The cutoff wavenumber m_c occurs at even higher values than its Eulerian counterpart, with the highest frequency band not yet rolling off at the 0.3 cpm resolution. When the semi-Lagrangian spectrum is integrated across frequencies (Fig. 6b), the resulting cumulative spectrum is similar to the Eulerian version (Fig. 5b), implying we are seeing the same physical process from two different perspectives.

6. Comparison of shear and strain variance

The Eulerian shear and strain fields can be compared to quantify the effects of vertical advection. Linear internal wave theory leads to a frequency-dependent relation for the vertical strain/shear variance ratio:

$$\frac{N^2\langle \eta_z^2\rangle}{\langle U_z^2\rangle} = \frac{(\omega^2 - f^2)}{(\omega^2 + f^2)} \frac{N^2}{(N^2 - \omega^2)}. \qquad (3)$$

Here f is the Coriolis frequency, and $\langle U_z^2\rangle = \langle (\partial u/\partial z)^2 + (\partial v/\partial z)^2\rangle$. Linear near-inertial waves have a low strain-to-shear variance ratio while waves with frequency near N have a high ratio. Comparison of linear theory to the measured ratio (Fig. 7) shows fair agreement at low wavenumbers ($m < 0.01$ cpm). The inertial band contains slightly too much strain at all wavenumbers. This could result from either high-frequency waves being Doppler-shifted to near-inertial encounter frequencies, or to nonlinear aspects of the wavefield. All other frequency bands exhibit too much shear variance at high wavenumbers to agree with linear theory. This could indicate that near-inertial waves (high-shear, low-strain) have been vertically Doppler-shifted to higher encounter frequencies, or that nonlinear effects are important at high frequencies.

The comparison in Fig. 7 suggests that the vertical self advection of the wave field is a key feature of the Eulerian observations. One wonders how the shear spectrum would appear using measurements made in a semi-Lagrangian frame. A hypothetical semi-Lagrangian shear spectrum has been created from the corresponding strain spectrum by assuming that the linear strain/shear variance ratio is valid. Since the theoretical ratio approaches zero at f, the estimate of semi-Lagrangian shear will be imprecise in the near-inertial band. The resulting hypothetical spectrum (Fig. 8a) is very similar to the semi-Lagrangian strain spectrum. When viewed in the frequency domain (Fig. 8b), most wavenumber bands exhibit an ω^{-2} slope in frequency, with only the highest wavenumber band (¼–½ cpm) showing disagreement.

It is worthwhile calling attention to the nonseparability at high wavenumber ($m > 0.1$ cpm) of both the semi-Lagrangian strain spectrum (Fig. 6a) and the hypothetical semi-Lagrangian shear spectrum (Fig. 8a). This departure from the GM model can be characterized by assigning a frequency dependence to the cutoff wavenumber m_c. This is seen to correspond to 10 m vertical scale at inertial frequency, increasing approximately as $(\omega/f)^{1/2}$ with increasing ω (Fig. 8a). To the extent that this tendency is correct, the GM hypothesis of separability is significantly in error, even in the semi-Lagrangian reference frame. Could the effects of horizontal advection be playing a role here? It is useful to create a simple model to estimate the roles of both vertical and horizontal advection.

7. Modeling the effects of vertical and horizontal advection

To replicate effects of vertical advection, we consider a GM-type model which is vertically advected by itself. The shear spectrum as observed in a semi-Lagrangian frame is modeled as:

$$\Phi(\omega, m) = E_0\omega^{-2} \frac{m^2}{m^2 + m_*^2} \frac{m_c^2}{m^2 + m_c^2}, \quad f < \omega < N \qquad (4)$$

where $m_* = 0.01$ cpm, and $m_c = 0.1$ cpm (Fig. 9, dark lines). Synthetic depth-time series of the semi-Lagrangian shear are created by assigning a random phase to each ω-m component before inverse-transforming ($64m$, 128ω components are used from 0.005–0.3 cpm, 0.008–1 cph). Ten independent time series are computed, each with a different set of random phases. A GM displacement field, $\eta(t)$, is similarly calculated, assuming a frequency spectral form, $=(\omega^2 - f^2)^{1/2}/\omega^3$, with rms displacement = 6 m. The simulated displacement field is uncorrelated with the shear field. This is justified since vertical displacement is dominated by low-mode internal waves, which are presumably uncorrelated with the high-wavenumber shear field. The ten semi-Lagrangian time series are vertically advected by $\eta(t)$. The time series as seen by a fixed observer, $du_0/dz(z, t) = du/dz(z - \eta(t), t)$, is cal-

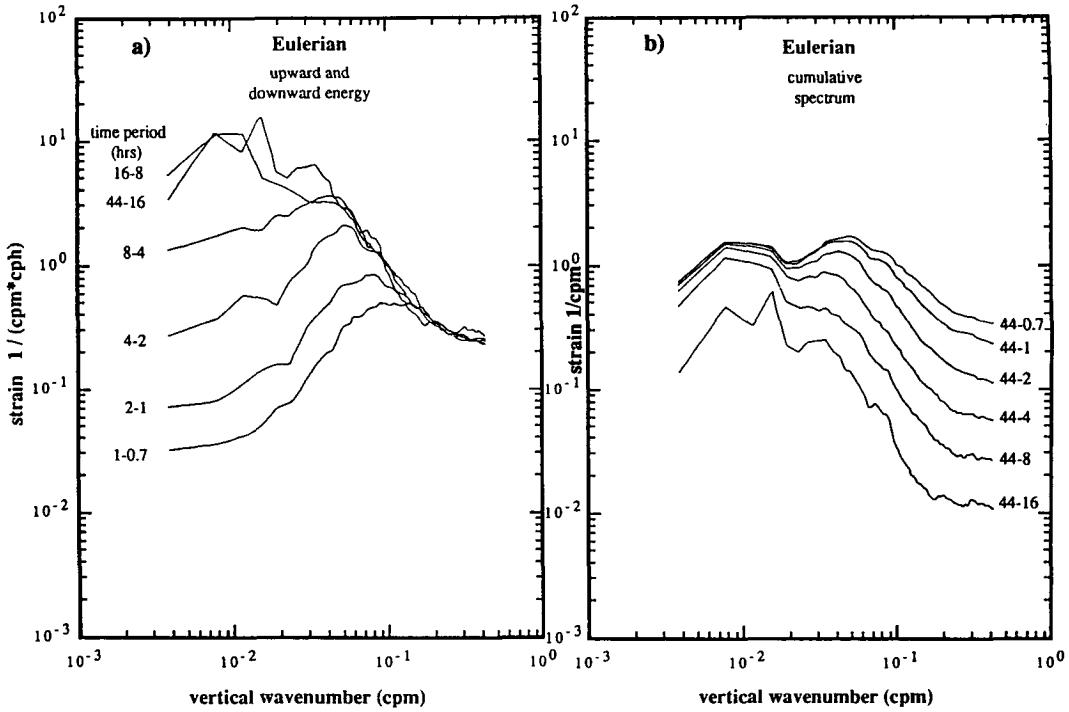

FIG. 5. (a) The PATCHEX Eulerian vertical strain (ω, m) spectrum is displayed in six different frequency bands, as in Fig. 4a. Spectral estimates have been logarithmically smoothed in m, with a bandwidth equal to $\delta m = \pm 0.1m$. (b) The cumulative strain spectrum's 44–0.7 hour band is very similar to the shear cumulative spectral value in Fig. 4d.

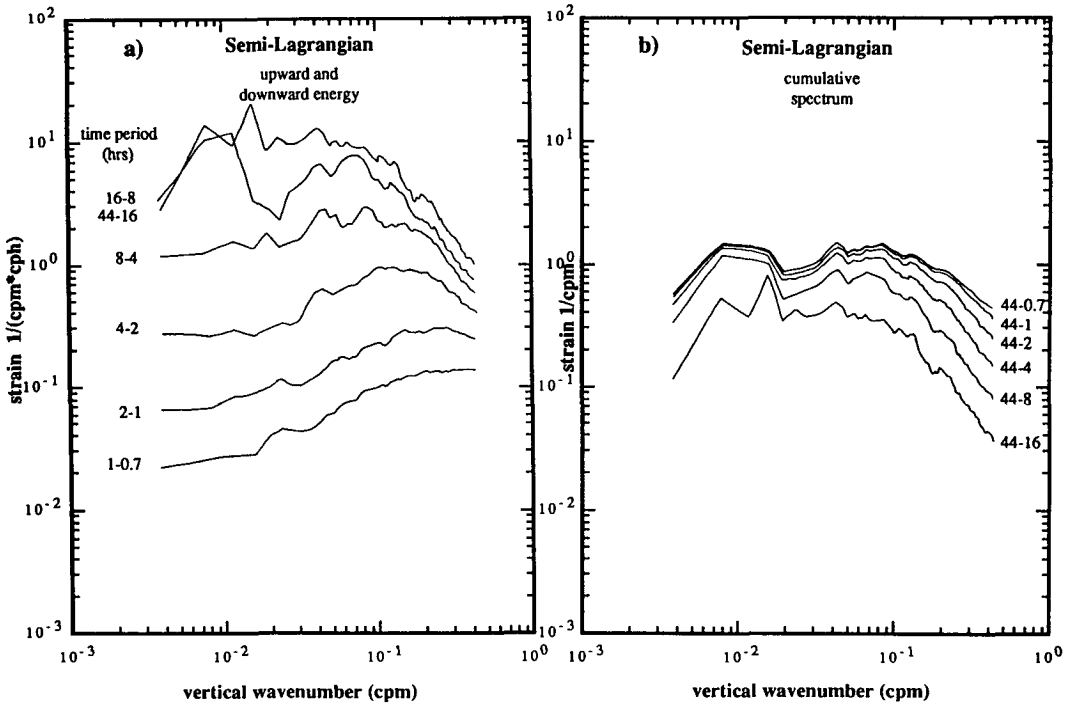

FIG. 6. The PATCHEX semi-Lagrangian vertical strain (ω, m) spectrum is shown in the same format as Fig. 5. Although the semi-Lagrangian spectrum in (a) looks quite different from the Eulerian strain spectrum in Fig. 5a, the semi-Lagrangian cumulative spectrum's 44–0.7 hour band (b) is very similar to the Eulerian (Fig. 5b).

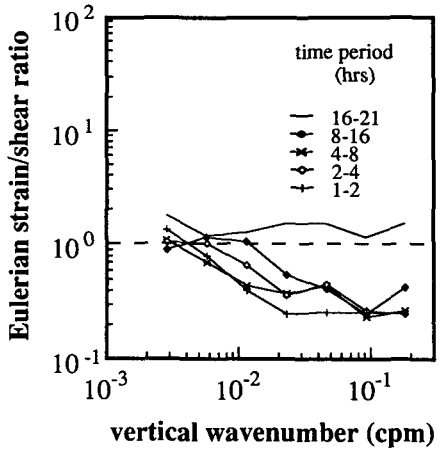

FIG. 7. The measured ratio of vertical strain/shear variance is divided by the ratio predicted by linear theory [Eq. (3)]. A value of 1 means perfect agreement, >1 too much strain, and <1 too little strain to agree with linear theory. Estimates are averaged in wavenumber to provide better precision.

culated. The average "vertically advected" spectrum (Fig. 9, light lines) exhibits characteristics similar to the observed Eulerian shear spectrum. Above $m = 0.1$ cpm, all frequencies bands have the same spectral level (white in ω), and m_c appears strongly frequency dependent.

Strain observations suggest that even in a semi-Lagrangian frame, a GM-like model still is not valid. A weak frequency dependence of the observed spectral cutoff, m_c, is seen. Could it be that horizontal advective effects are contaminating our semi-Lagrangian observations?

One can take a similar approach to study the effects of horizontal advection on the semi-Lagrangian reference frame. Equation (4) is used to derive the shear field, again simulated with $64m$, 128ω components from 0.005–0.3 cpm, 0.008–1 cph. This time only horizontal advection is considered, presumably caused by a velocity field dominated by large vertical scales [$u \neq u(z)$]. Here, a frequency dependence of ω^{-2} for $f < \omega < N$ is assumed and $u(t)$ is integrated to give a

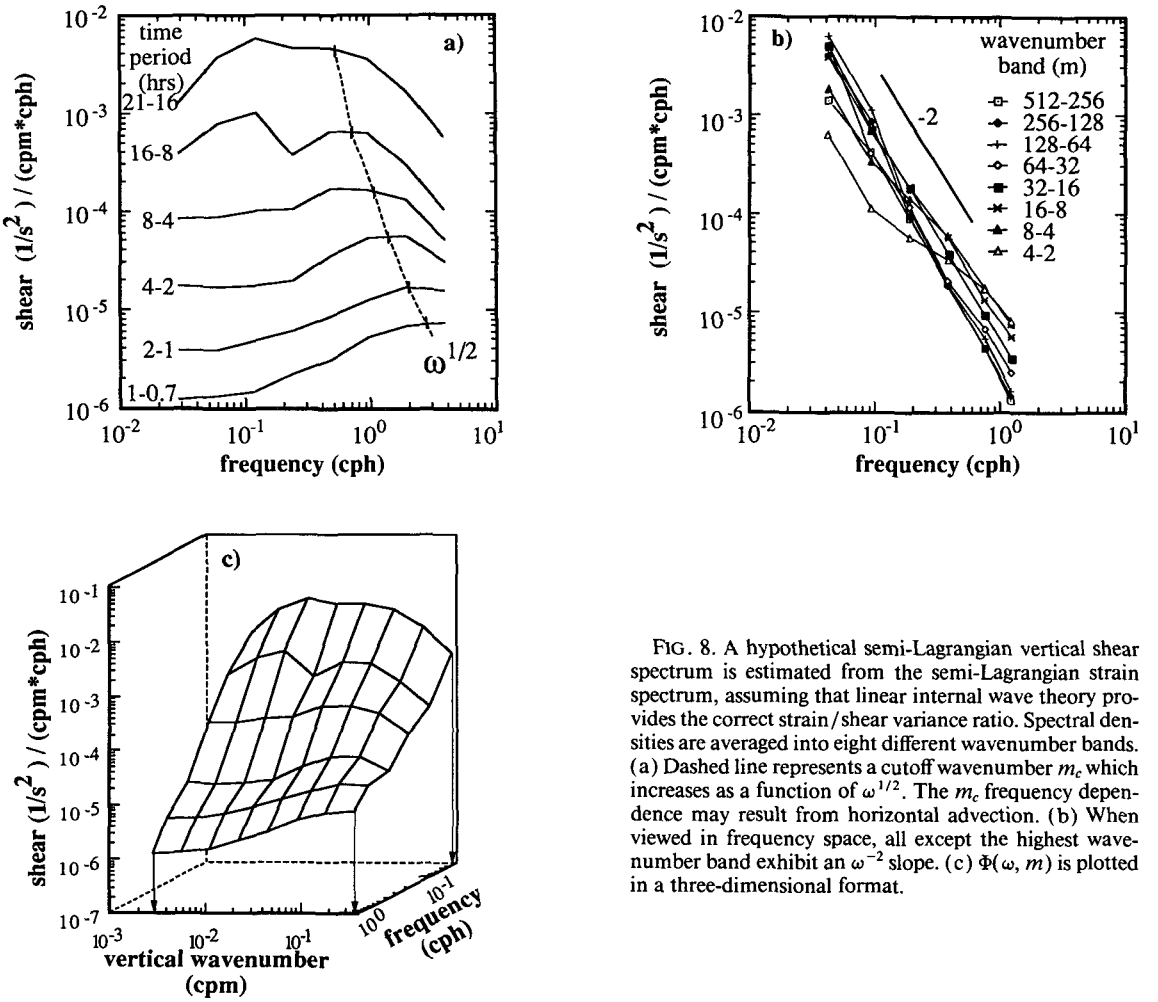

FIG. 8. A hypothetical semi-Lagrangian vertical shear spectrum is estimated from the semi-Lagrangian strain spectrum, assuming that linear internal wave theory provides the correct strain/shear variance ratio. Spectral densities are averaged into eight different wavenumber bands. (a) Dashed line represents a cutoff wavenumber m_c which increases as a function of $\omega^{1/2}$. The m_c frequency dependence may result from horizontal advection. (b) When viewed in frequency space, all except the highest wavenumber band exhibit an ω^{-2} slope. (c) $\Phi(\omega, m)$ is plotted in a three-dimensional format.

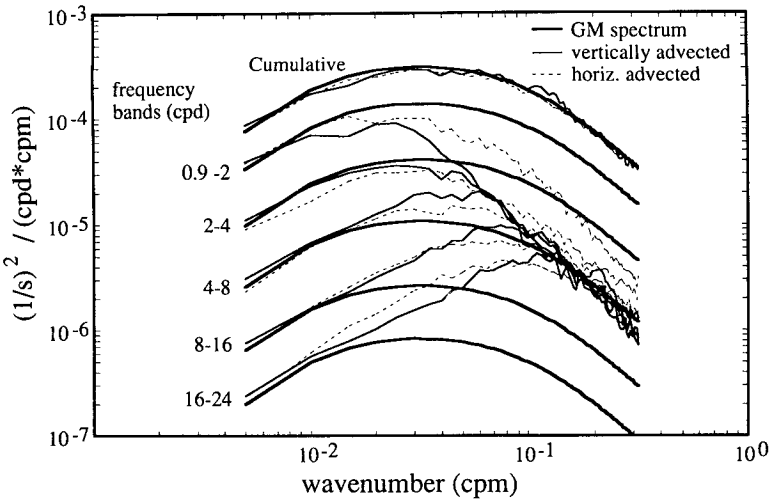

FIG. 9. Simulated time series of the Garrett–Munk shear spectrum (dark lines) have been horizontally and vertically advected past a fixed observer. Vertical advection is simulated from the GM spectrum. The resultant spectrum (light lines) displays many of the same characteristics of Fig. 4a. Above 0.1 cpm Doppler-shifting is so strong that the dominant near-inertial input spectrum has been redistributed across all frequency bands, producing a white frequency spectrum. The cumulative spectrum (integrated across all frequencies, top line) confirms that the advected time-series has the same wavenumber distribution, although a quite different frequency dependence at high wavenumbers. Dashed lines represent the simulated spectrum when only horizontal advection is present. It also suffers from Doppler-contamination, with low frequencies less affected due to their larger horizontal length-scales.

horizontal displacement time series $X(t)$, with O(600 m) rms motions. The assumption that $X(t)$ is independent of depth is inaccurate, but should not affect the high-wavenumber observations, which experience a uniform velocity over their vertical length scales. The semi-Lagrangian observed field is calculated from $du_0/dz(x_0, z, t) = du/dz(x_0 + X(t), z, t)$. It is assumed that the GM-like shear model [Eq. (4)] is applicable to the purely Lagrangian frame.

This simple advection model ignores nonlinear interactions between the high wavenumber waves and the background velocity field (i.e., no critical layers present!). The neglect of the dynamics of the wave field is a significant feature of the model. However, it is useful to explore the aspects of the observed spectra that result from simple kinematic considerations, prior to developing a dynamical model which attempts to explain the spectral form. Ten simulated time series were calculated, with the resultant spectrum (Fig. 9, dashed lines) showing strong Doppler-smearing at high wavenumbers. Lower frequencies, which have larger horizontal wavelengths, are less affected (i.e., 0.9–2 cpd band). For a linear internal wave with horizontal wavenumber k advected by velocity u, the Doppler-shifted frequency ω' is given by $\omega' = \omega + ku = \omega + um(\omega^2 - f^2)^{1/2}/N$, for $\omega \ll N$. Near-inertial waves suffer little Doppler-shifting from horizontal advection.

The simulated spectrum exhibits a cutoff wavenumber m_c that is frequency-dependent. The observed frequency dependence of m_c in the semi-Lagrangian strain and hypothetical shear spectrum (Fig. 8a) could be an artifact of horizontal advection. Note that the hypothetical semi-Lagrangian shear spectrum (Fig. 8a) shows less Doppler-smearing at high wavenumbers than the above model (Fig. 9). This could arise if *FLIP* was actually tracking the horizontal velocity field. This is unlikely. *FLIP*'s motions are determined by wind forcing on the 20 m superstructure, combined with mixed layer and upper thermocline velocities acting on the 90 m draft, all constrained by the two-point moor. Furthermore, strain has been calculated between 150 and 406 m depth, which should not have horizontal velocities highly correlated to *FLIP*'s motions. Alternatively, the true "unadvected" spectrum may have a different form than that of (4), with more energy at lower frequencies for high wavenumbers. A steeper spectral slope could arise due to critical layer processes, triad-interactions, or increased vortical (cyclogeostrophic) motions with large horizontal length scales.

8. Richardson function estimates

What are the implications of the Eulerian and semi-Lagrangian shear spectra on the temporal scales of low Ri events? Ri^{-1} is now defined as a function of ω (as in Pinkel 1985):

$$\mathrm{Ri}^{-1}(\omega, m) = \frac{1}{N^2}\int_0^{\omega} d\omega \int_0^{m} \Phi(\omega, m)dm \quad (5)$$

and is computed from both viewpoints (Fig. 10). The Eulerian Ri^{-1} suggests that most of the high wavenumber variance results from high frequency motions, with near-inertial, high wavenumber waves contributing little to the overall variance. In comparison, the simulated semi-Lagrangian Ri^{-1} suggests that half of the shear variance comes from near-inertial motions. Measurements from fixed-depth sensors mistakenly indicate that high-frequency motions provide most of the shear at high wavenumbers. This suggests that the near-inertial field plays little role in causing instabilities. However, isopycnal-following sensors see half of the total shear variance resulting from near-inertial motions, indicating that high vertical wavenumber, near-inertial waves can play an important role in low Ri events.

9. Conclusions

Historically it has been difficult to reconcile observations of vertical and horizontal motion in the sea using linear internal wave dynamics (Muller et al. 1978). The concept of "finestructure contamination" (Phillips 1971; Garrett and Munk 1971) as well as the notion of an additional class of vortical (or cyclogeostrophic) motions (Muller et al. 1978; Muller 1984; Muller et al. 1988) have been introduced to help reconcile linear internal wave theory with observation. Discrepancy with linear theory is particularly acute when shear and strain (rather than velocity or displacement) fields are considered. These are dominated by the high vertical wavenumber constituents. The advection of these small scale features by the more energetic large scale motions strongly influences observations.

In this work, measurements of the time evolution of fine-scale shear and strain have been presented. The initial objective was to augment the one-dimensional view of the shear field previously obtained using dropsonde sensors. It is found, not surprisingly, that as progressively finer vertical scales are considered, the Eulerian time evolution of the shear becomes more strongly influenced by vertical advection. This is inferred through comparison with wavenumber–frequency spectra of vertical strain. In an Eulerian frame, strain is defined as the ratio of instantaneous to mean density gradient. This definition replicates aspects of the "finestructure contamination" problem shared with the sonar-derived shear measurements. Those aspects of the Eulerian strain and shear spectra which are uniformly influenced by vertical advection agree in many details. Agreement with linear internal wave theory is poor, as the observed wave frequency presumably differs from intrinsic frequency, particularly at small vertical scale.

In an isopycnal-following frame, strain is defined as the ratio of instantaneous to mean isopycnal separation, minus 1. The observations are presumably unaffected by vertical displacement. When well-known discrepancies in near inertial, tidal, and near Väisälä frequency bands are neglected, Pinkel (1975, 1983), the semi-Lagrangian observations are in much better agreement with existing wavefield models (Garrett and Munk 1972, 1975, 1979). In particular, the key as-

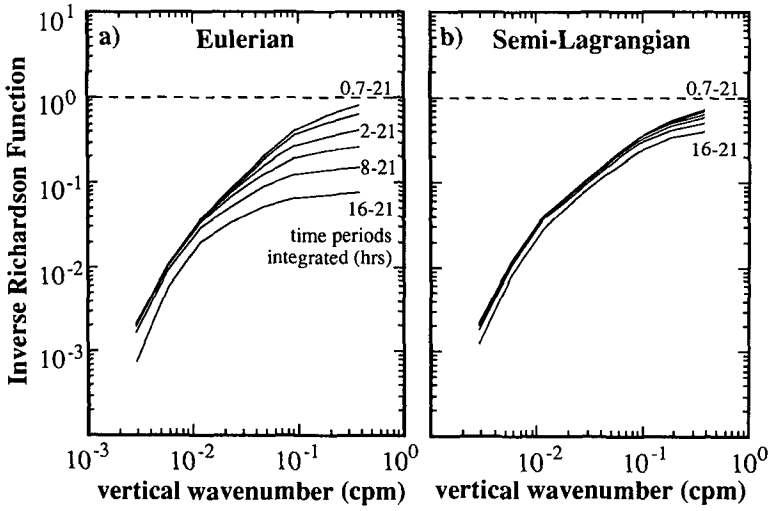

FIG. 10. Estimates (a) of Ri^{-1} based on the Eulerian shear spectrum (Fig. 4) and derived (b) from the hypothetical semi-Lagrangian spectrum (Fig. 8). The semi-Lagrangian Ri^{-1} shows the near-inertial band contributing nearly half of the total variance, whereas the contaminated Eulerian Ri^{-1} mistakenly estimates that the near-inertial band provides only 10% of the overall variance.

sumption—that the frequency and wavenumber dependencies of the spectrum are separable—is more nearly valid in the semi-Lagrangian frame. The principal remaining discrepancy, that the high wavenumber spectral cutoff, m_c, appears to be a weak function of frequency, might be associated with horizontal advective effects.

The Gargett et al. (1981) wavenumber spectral model agrees well with the PATCHEX dataset. A low-wavenumber rolloff should perhaps be included, suggesting a spectral shape which is band-limited between m = 0.01–0.1 cpm. This is equivalent to choosing a higher value of j_* in the GM model (Munk 1981).

Gargett et al. suggest $\mathrm{Ri}^{-1}(m_c) = 1$, while the PATCHEX dataset has $\mathrm{Ri}^{-1}(m_c) \approx 0.3$. This is in closer agreement with Munk's (1981) value of $\mathrm{Ri}^{-1}(m_c) = 0.5$. Duda and Cox (1989) found $\mathrm{Ri}^{-1}(m_c) = 1$–3. Taken together with our measurements, the implication is that m_c is not necessarily determined by Ri^{-1} (that is, the background shear level does not set the high wavenumber cutoff). The kinematic self-distortion of the wavefield must play an important role.

The interpretation of Ri^{-1} is quite different for the two frames of reference. The Eulerian Ri^{-1} suggests that high-frequency motions are responsible for low Ri events. The semi-Lagrangian Ri^{-1} indicates that near-inertial waves contribute half of the overall variance.

Acknowledgments. The authors would like to thank Mike Goldin, Lloyd Green, and Eric Slater for their engineering expertise in developing and operating the instruments. During PATCHEX, *FLIP* was professionally operated by Captain Dewitt Efird and crew. This work was funded by the Office of Naval Research, Code 1120 under Contract N00014-90-J-1099; and the National Science Foundation, Contract NSF OCE 87-11936.

APPENDIX

Bias in Velocity Due to Beam Separation

Consider the simplified case of a single wave component with north–south horizontal wavenumber k in an ocean of uniform stratification. The velocity field is specified by

$$(u, v, w) = V_0\left(i\frac{f}{\omega}, 1, -\frac{k}{m}\right)e^{i(ky+mz-\omega t)}. \quad \text{(A1)}$$

Let θ equal the downward angle of the sonar beams, such that along-beam velocity becomes [from Eq. (2)]:

$$v_n = V_0 e^{i(ky_n+mz-\omega t)}\left(\sin\theta - \frac{k}{m}\cos\theta\right)$$

$$v_s = V_0 e^{i(ky_s+mz-\omega t)}\left(-\sin\theta - \frac{k}{m}\cos\theta\right) \quad \text{(A2)}$$

where y_n and y_s are the horizontal locations of the return signal. Define Δy as half the distance between beams: $\Delta y = (y_s - y_n)/2 = z/\tan\theta$ (z = depth from sonar). The estimated horizontal velocity $\hat{v}$ is given by

$$\hat{v} = \frac{v_n - v_s}{2\sin\theta} = \frac{V_0}{2}e^{i(ky_n+mz-\omega t)}\left[(1 + e^{i2k\Delta y}) - \frac{k}{m}\cot\theta(1 - e^{i2k\Delta y})\right]. \quad \text{(A3)}$$

The correct velocity is $V_0 e^{i(mz-\omega t)}$. The estimate is in error in both magnitude and phase. Whereas phase error will bias temporal correlations with other parameters, it will not affect spectral densities. The variance bias B is given by

$$B = \frac{\hat{v}^*\hat{v}}{v^*v} = \frac{1}{2}[(1 + b^2) + (1 - b^2)\cos\phi] \quad \text{(A4)}$$

where $b = (k/m)\cot\theta$, and $\phi = 2k\Delta y$. For internal waves with $\omega \ll N$, $k/m \approx (\omega^2 - f^2)^{1/2}/N$. During PATCHEX, N = 5.3 cph for the short-range sonar. Spectral estimates are made for $\omega < 1$ cph, allowing us to assume $b^2 \ll 1$, reducing (A4) to

$$B = \cos^2(k\Delta y) = \cos^2\left[\frac{mz(\omega^2 - f^2)^{1/2}}{N\tan\theta}\right]. \quad \text{(A5)}$$

This is simply the response function expected by ignoring w's contribution in (A2). Equation (A5) is valid for both horizontal velocity and vertical shear.

We can approximate the spectral bias for a specified ω, m by integrating B over all z, giving

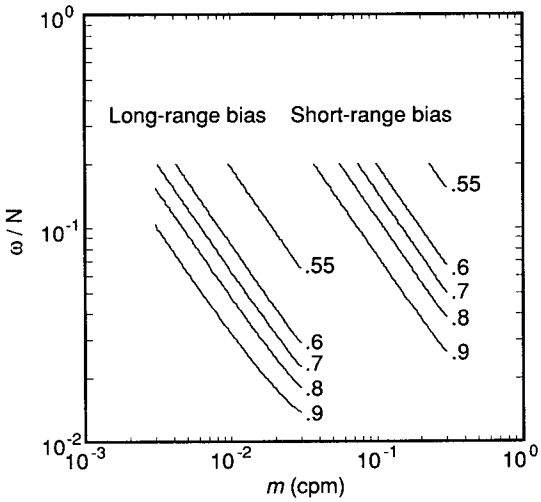

FIG. A1. *Estimated bias in spectral variance.* The finite separation between beam components leads to an underestimate of the actual velocity variance (N/f = 100). This bias, F, is negligible for low wavenumbers and near-inertial frequencies; F is dependent upon the product ωm at mid-frequencies. It asymptotes to 50% of the true variance at high ωm. Estimates are shown for both the short-range and long-range sonars, assuming horizontal isotropy.

$$F(\omega, m) = \frac{1}{z_{\max}} \int_0^{z_{\max}} B(\omega, m, z)dz = \frac{1}{2} + \frac{N \tan\theta}{4(\omega^2 - f^2)^{1/2} m z_{\max}} \sin\left(\frac{2(\omega^2 - f^2)^{1/2} m z_{\max}}{N \tan\theta}\right). \quad \text{(A6)}$$

For an internal wave with horizontal wavenumber K traveling in horizontal direction ψ, (A5) and (A6) are modified by setting $k = K \sin\psi$. Assuming an isotropic wave field, $F(\omega, m)$ can be numerically averaged over all ψ, yielding Fig. A1. $F(\omega, m)$ asymptotes to 0.5, and is dependent upon the product ωm over mid-frequencies. At the long-range sonar's highest resolution (0.03 cpm), $\omega > 0.07N$ will be attenuated by 55%. At 0.03 cpm, the short-range sonar suffers little bias over all ω. At its highest resolution (0.3 cpm), it suffers 55% attenuation for $\omega > 0.2N$.

By integrating $F(\omega, m)$ over all ω, the overall bias for a given wavenumber m can be estimated. If the velocity field has an ω^{-2} spectral form, which contains half its variance between f-2f (which is the frequency range with small bias), the estimated overall velocity bias is not severe. For instance, the long-range sonar would underestimate velocity variance by 20% at 0.03 cpm, while the short-range sonar would suffer 10% bias at 0.3 cpm.

REFERENCES

Desaubies, Y., and W. K. Smith, 1982: Statistics of Richardson number and instability in oceanic internal waves. *J. Phys. Oceanogr.*, **12,** 1245–1259.

Duda, T. F., and C. S. Cox, 1989: Vertical wave number spectra of velocity and shear at small internal wave scales. *J. Geophys. Res.*, **94,** 939–950.

Gargett, A. E., P. J. Hendricks, T. B. Sanford, T. R. Osborn and A. J. Williams, 1981: A composite spectrum of vertical shear in the upper ocean. *J. Phys. Oceanogr.*, **11,** 1258–1271.

Garrett, C. J. R., and W. H. Munk, 1971: Internal wave spectra in the presence of fine-structure. *J. Phys. Oceanogr.*, **1,** 196–202.

—— and ——, 1972: Space-time scales of internal waves. *Geophys. Fluid Dyn.*, **2,** 225–264.

—— and ——, 1975: Space-time scales of internal waves: a progress report. *J. Geophys. Res.*, **80,** 291–297.

—— and ——, 1979: Internal waves in the ocean. *Ann. Rev. Fluid Mech.*, **11,** 339–369.

Gregg, M. C., 1989: Scaling turbulent dissipation in the thermocline. *J. Geophys. Res.*, **94,** 9686–9698.

Holloway, G., 1980: Oceanic internal waves are not weak waves. *J. Phys. Oceanogr.*, **10,** 906–914.

Kunze, E., A. J. Williams, III and M. G. Briscoe, 1990: Interpreting shear and strain finestructure from a neutrally-buoyant float. *J. Geophys. Res.*, **95,** 18 111–18 125.

Lhermitte, R., and R. Serafin, 1984: Pulse-to-pulse coherent Doppler sonar signal processing techniques. *J. Atmos. Oceanic Technol.*, **1,** 293–308.

Muller, P., 1984: Small-scale vortical motions. *Internal gravity waves and small-scale turbulence, Proc., 'Aha Huliko'a Hawaiian Winter Workshop,* P. Muller and R. Pujalet, Eds., Hawaii Institute of Geophys., Spec. Pub., 249–262.

——, D. J. Olbers and J. Willebrand, 1978: The IWEX spectrum. *J. Geophys. Res.*, **83,** 479–500.

——, R. Lien and R. Williams, 1988: Estimates of potential vorticity at small scales in the ocean. *J. Phys. Oceanogr.*, **18,** 401–416.

Munk, W. H., 1981: Internal waves and small scale processes. *Evolution of Physical Oceanography,* B. Warren and C. Wunsch, Eds., The MIT Press, 264–291.

Phillips, O. M., 1971: On spectra measured in an undulating layered medium. *J. Phys. Oceanogr.*, **1,** 1–6.

Pinkel, R., 1975: Upper ocean internal wave observations from FLIP. *J. Geophys. Res.*, **80,** 3892–3910.

——, 1983: Doppler sonar observations of internal waves: Wavefield structure. *J. Phys. Oceanogr.*, **13,** 804–815.

——, 1985: A wavenumber–frequency spectrum of upper ocean shear. *J. Phys. Oceanogr.*, **15,** 1453–1469.

——, A. Plueddemann and R. Williams, 1987: Internal wave observations from FLIP in MILDEX. *J. Phys. Oceanogr.*, **17,** 1737–1757.

——, J. Sherman, J. Smith and S. Anderson, 1991: Strain: observations of the vertical gradient of isopycnal vertical displacement. *J. Phys. Oceanogr.*, submitted.

Plueddemann, A. J., 1987: Observations of the upper ocean using a multibeam Doppler sonar. Ph.D. dissertation, University of California, San Diego, 183 pp.

Sherman, J. T., 1989: Observations of fine-scale vertical shear and strain in the upper ocean. Ph.D. dissertation, University of California, San Diego, 145 pp.

Williams, R. G., 1985: The internal tide off Southern California. Ph.D. dissertation, University of California, San Diego, 169 pp.